



Article

Analysis and Evaluation of Fiber Orientation Reconstruction Methods

Kevin Breuer ^{1,*}, Markus Stommel ¹ and Wolfgang Korte ²

¹ TU Dortmund University, Mechanical Engineering, Chair of Plastics Technology, Leonhard-Euler-Str. 5, 44227 Dortmund, Germany

² PART Engineering GmbH, Friedrich-Ebert-Straße 75, 51429 Bergisch Gladbach, Germany

* Correspondence: kevin.breuer@tu-dortmund.de

Received: 24 May 2019; Accepted: 1 July 2019; Published: 4 July 2019



Abstract: The calculation of the fiber orientation of short fiber-reinforced plastics with the Fokker–Planck equation requires a considerable numerical effort, which is practically not feasible for injection molding simulations. Therefore, only the fiber orientation tensors are determined, i.e., by the Folgar–Tucker equation, which requires much less computational effort. However, spatial fiber orientation must be reconstructed from the fiber orientation tensors in advance for structural simulations. In this contribution, two reconstruction methods were investigated and evaluated using generated test scenarios and experimentally measured fiber orientation. The reconstruction methods include spherical harmonics up to the 8th order and the method of maximum entropy, with which a Bingham distribution is reconstructed. It is shown that the quality of the reconstruction depends massively on the original fiber orientation to be reconstructed. If the original distribution can be regarded as a Bingham distribution in good approximation, the method of maximum entropy is superior to spherical harmonics. If there is no Bingham distribution, spherical harmonics is more suitable due to its greater flexibility, but only if sufficiently high orders of the fiber orientation tensor can be determined exactly.

Keywords: maximum entropy; spherical harmonics; fiber orientation; ODF; reconstruction; injection molding

1. Introduction

Short fiber-reinforced plastics are ideal materials for high-performance lightweight applications. This usually requires a very accurate numerical determination of the mechanical stresses by structural simulations during the engineering process of technical products. This can be a major challenge: If short glass fiber reinforced thermoplastics are processed by injection molding or other primary forming processes, there is a direct correlation between the resulting mechanical properties of the material and the manufacturing process. This is caused by locally different microstructures, since the spatial orientation of the short fibers of the composite material varies at each point of the molded part depending on the flow conditions over time during the manufacturing process. Therefore, it is obvious to describe the mechanical behavior of the component as a function of the fiber orientation. Consequently, the more precisely the fiber orientation can be modelled, the more precisely the mechanical design of the molded part can be performed.

In injection molding simulation, the mathematical description of the fiber orientation is significantly simplified due to the very high numerical effort required otherwise. Reconstruction methods are used to recover the original fiber orientation in a post-processing step from the orientation tensor. In this paper, the performance of two reconstruction methods was compared and analyzed. The reconstruction methods involved the spherical harmonics and the maximum entropy method. The analysis was

performed as follows: Test scenarios were developed, and the fiber orientation was calculated using both reconstruction methods. A subsequent comparison between reconstructed and original fiber orientation shows the quality of the reconstruction as well as its calculation effort. The developed test scenarios allowed the comparison of the two reconstruction methods for a much larger spectrum of different fiber orientation compared to experimental tests of injection molded specimens. Furthermore, it is possible to evaluate the reconstruction methods independently from any process simulation.

The aim of this paper was to show the advantages and disadvantages of the individual reconstruction methods.

2. Fiber Orientation

The orientation of a single fiber in space can be given as a direction vector \mathbf{p} in spherical coordinates on the unit sphere \mathbb{S} (see Figure 1). Here, the angle θ is defined as between 0 and π , and ϕ between $-\pi$ and π .

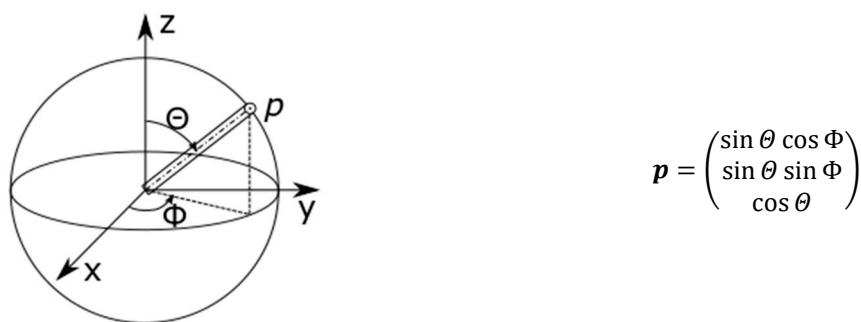


Figure 1. Orientation of single fiber in spherical coordinates.

The change of the orientation \mathbf{p} of a fiber in a fluid–fiber suspension of velocity \mathbf{u} can be modeled basically with Jeffrey's equation [1]. Jeffrey describes the movement of ellipsoidal particles in a viscous fluid under the condition of a laminar flow. For a Newtonian fluid without externally applied moments, the change of the orientation \mathbf{p} is:

$$\dot{\mathbf{p}} = -\boldsymbol{\omega} \cdot \mathbf{p} + \lambda [\boldsymbol{\varepsilon} \cdot \mathbf{p} - \boldsymbol{\varepsilon} : (\mathbf{p} \otimes \mathbf{p}) \mathbf{p}], \quad (1)$$

The vorticity tensor $\boldsymbol{\omega}$ is calculated by:

$$\boldsymbol{\omega} = \frac{1}{2} (\nabla \mathbf{u}^T - \nabla \mathbf{u}), \quad (2)$$

and the strain rate tensor $\boldsymbol{\varepsilon}$ with:

$$\boldsymbol{\varepsilon} = \frac{1}{2} (\nabla \mathbf{u}^T + \nabla \mathbf{u}). \quad (3)$$

The constant:

$$\lambda = \frac{a_r^2 - 1}{a_r^2 + 1}, \quad (4)$$

is the fiber geometry factor, which is determined by the fiber aspect ratio $a_r = \frac{l}{d}$ of fiber length l and fiber diameter d . In a simple shear flow, the solution of the Jeffrey equation is periodic in time. This means that after some time, a single fiber rotates back to its initial position. Jeffrey's equation is a useful model for the calculation of fiber orientation in the case of a thin suspension [2]. Thin means in this case that the fibers can statistically rotate undisturbed in the suspension. For suspensions with higher fiber concentrations as typically occur in technical relevant short-fiber reinforced plastics, fiber interaction plays an important role. Hence, Jeffery's equation alone is not applicable here. The suspensions can be

classified according to the fiber volume content v_F and the aspect ratio a_r [2]. The classification is listed in Table 1.

Table 1. Classification of fluid–fiber suspensions.

Regime	Volume Fraction: v_F
Dilute	$v_f < \frac{1}{a_r^2}$
Semi-Dilute	$\frac{1}{a_r^2} < v_F < \frac{1}{a_r}$
Concentrated	$\frac{1}{a_r} > v_F$

In technical applications, typically, there are between 2000 and 20,000 fibers per cubic millimeter, depending on the fiber volume content. Therefore, a deterministic consideration of the fiber orientation of each individual fiber is not feasible due to this large number, and a statistical analysis is carried out accordingly. The fiber orientation density function (ODF) $\psi(\mathbf{p})$ is defined for all fibers in the unit sphere. It indicates the probability of a fiber pointing in a certain direction \mathbf{p} . The ODF is periodic, i.e., $\psi(\mathbf{p}) = \psi(n\pi\mathbf{p})$, $n \in \mathbb{N}$ applies. Furthermore, a normalization condition is given by:

$$\psi = \oint_{\mathbb{S}} \psi(\Theta, \Phi) d\mathbb{S} = \int_0^{2\pi} \int_0^\pi \psi(\Theta, \Phi) \sin \Theta d\Theta d\Phi = 1 \quad (5)$$

The statistical consideration of the fiber orientation allows the use of the so-called Fokker–Plank equation for the calculation. The Fokker–Planck equation generally describes the change of a distribution function of fluctuating macroscopic variables [3]. The first application of the Fokker–Planck equation was to calculate the Brownian motion [4]. In its simplest, one-dimensional form, the Fokker–Plank equation is given by:

$$\frac{\partial W}{\partial t} = \left[-\frac{\partial}{\partial x} D^{(1)}(x) + \frac{\partial^2}{\partial x^2} D^{(2)}(x) \right] W. \quad (6)$$

W is a distribution function, depending on a variable x . The variable $D^{(1)}$ is called the drift part and $D^{(2)}$ the diffusion part. Both the drift and diffusion part can be determined on the basis of the microscopic behavior or derived from the statistical behavior on the macroscopic level. In the context of fiber orientation, the drift part corresponds to the part induced by hydrodynamic forces, and the diffusion part corresponds to the fiber interaction. To calculate the ODF, Jeffrey's equation can be used for the drift part of the Fokker–Plank equation. For the diffusion part, an approach for fiber interaction with:

$$D_r = C_i |2\varepsilon|, \quad (7)$$

is used. The Fokker–Planck equation for an ODF $\psi(\mathbf{p})$ therefore results in:

$$\frac{\partial \psi}{\partial t} = -\nabla \cdot (\dot{\mathbf{p}}\psi) + D_r \nabla^2 \psi. \quad (8)$$

Solving the Fokker–Plank equation within the framework of an injection molding simulation is numerically very costly, since the differential equation has to be solved in 3D space on the unit sphere \mathbb{S} . One possibility to reduce the computational effort is to decompose the ODF into moments of spherical harmonics. These moments are also known as fiber orientation tensors:

$$\mathbf{a}_N = a_{ijklmn\dots} = \int_0^{2\pi} \int_0^\pi p_i p_j p_k p_l p_m p_n p_{\dots} \psi(\Theta, \Phi) \sin \Theta d\Theta d\Phi. \quad (9)$$

Folgar and Tucker apply the decomposition to the Fokker–Planck equation [5]. For the second-order fiber orientation tensor, the resulting equation reads:

$$\frac{\partial a_{ij}}{\partial t} = -\frac{1}{2}(\omega_{ik} \cdot a_{kj} - a_{ik} \cdot \omega_{kj}) + \frac{\lambda}{2}[\varepsilon_{ik} \cdot a_{kj} + a_{ik} \cdot \varepsilon_{kj} - 2\varepsilon_{kl}a_{ijkl}] + 2D_r(\delta_{ij} - 3a_{ij}). \quad (10)$$

It should be noticed that the second-order orientation tensor depends on the fourth-order fiber orientation tensor a_{ijkl} . Analogously, the fourth-order fiber orientation tensor can be calculated with:

$$\frac{\partial a_{ijkl}}{\partial t} = -(\omega_{im} \cdot a_{mjkl} - a_{ijkm} \cdot \omega_{ml}) + \lambda[\varepsilon_{im} \cdot a_{mjkl} + a_{ijkm} \cdot \varepsilon_{ml} - 2\varepsilon_{mn}a_{ijklmn}] + D_r(-20a_{ijkl} + 2(a_{ij}\delta_{kl} + a_{ik}\delta_{jl} + a_{il}\delta_{jk} + a_{jk}\delta_{il} + a_{ji}\delta_{ik} + a_{kl}\delta_{ij})). \quad (11)$$

Hereby, a dependency on the fiber orientation tensor of the next higher even-order a_{ijklmn} has to be considered. In order to solve the Folgar–Tucker equation, it is necessary to calculate the fiber orientation tensor of the next higher even order using an approximation. So-called closures offer the possibility for this purpose. Due to the fact that higher-order tensors contain, in principle, more information than lower-order tensors, a closure can only be based on assumptions. A list, including references, for further information of known closures for the fourth-order tensor is given in Table 2 and for the sixth order in Table 3.

Table 2. List of closures for fourth-order fiber orientation tensor.

Closure Name	Reference
Linear	[6,7]
Quadratic	[7–9]
Hybrid	[7,10]
Exact	[11]
Fast Exact (FEC)	[11,12]
Bingham	[13]
Orthotropic	[10,14]
Natural	[15]
Neural Network (NNET)	[16]
Neural Network Orthotropic (NNORT)	[17]
Quad R	[18]
Hinch and Leal W1 (isotropic)	[19]
Hinch and Leal S2 (strong flow)	[19]
Hinch and Leal HL1	[18]
Hinch and Leal HL2	[18]
Hinch and Leal HL1Q	[18]
Invariant Based optimal fitting (IOBF)	[20]

Table 3. List of closures for sixth-order fiber orientation tensor.

Closure Name	Reference
Linear	[7]
Quadratic	[7,21]
Hybrid	[7]
Invariant Based	[22]

The large number of closures developed and discussed in the literature shows that it is not evident to develop a comprehensive closure that is both numerically efficient and satisfactorily accurate. Commercial injection molding simulation programs usually use the hybrid or orthotropic closures for the fourth-order tensor [23,24], although it can be shown that more accurate closures exist [10].

Not only is the accuracy of the closures discussed in the literature, but also the results of process simulations are a subject of many research projects. However, the second- and the fourth-order fiber orientation tensors are often used as the evaluation parameter and not the ODF—for example, in the work on the influence of fiber interaction [10,25], or for the processing of long fibers [26]. Even in the work by Férec et al. [27], in which the Fokker–Planck equation is solved, the fiber orientation tensors and not the ODF were used as evaluation criteria. Russel et al. investigated the prediction of the fiber orientation tensor in fused filament fabrication [28], while Kuhn et al. in compression molding of long fibers.

However, the design process of components often requires the use of the ODF $\psi(p)$ and not only the fiber orientation tensors, i.e., structural simulations by the finite element method, generating a representative volume element (RVE) or calculating the effective stiffness C_{eff} using a two-step homogenization [29]:

$$C_{eff} = \oint C(p)\psi(p)dp. \quad (12)$$

Müller and Böhlke showed that the two-stage tensor is not sufficient to describe a microstructure in order to determine effective composite properties with sufficient accuracy [30]. Therefore, it is absolutely necessary to investigate the quality of the reconstruction methods of an ODF on the basis of a fiber orientation tensor.

Due to the necessary knowledge of the ODF, a reconstruction problem arises, how an ODF can be derived from the fiber orientation tensor. This problem is ruled by the fact that the reconstruction of the ODF from the fiber orientation tensors is not unambiguous, as Figure 2 illustrates. It shows two different ODFs: on the one hand, an ODF with planar isotropy, and on the other hand, one with unidirectional distribution of two equal maxima. The red color on the shown unit spheres indicates a high fiber probability density. The second-order fiber orientation tensors belonging to these two different ODFs are identical. This example explains that by knowing exclusively the fiber orientation tensor, there can be no unambiguous reconstruction of the ODF. Mathematically speaking, the reconstruction problem is ill-posed.

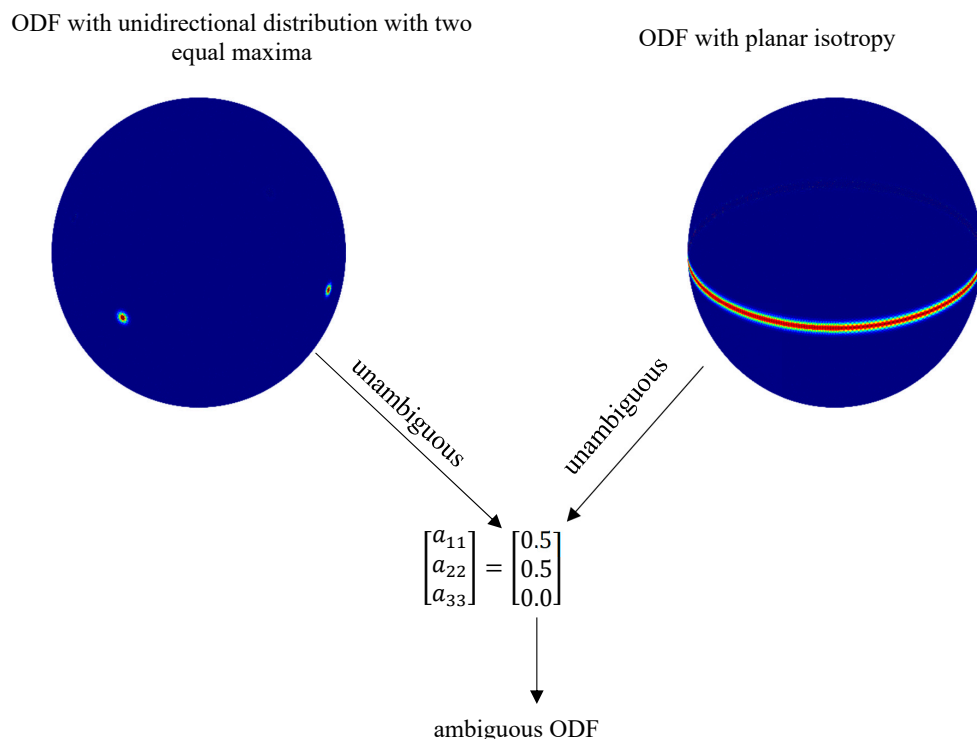


Figure 2. Two different orientation density functions (ODFs) (left: unidirectional with two maxima, right: planar isotropy) with the same fiber orientation tensor to illustrate the ambiguity of the reconstruction.

3. Icosphere

A discretization of the unit sphere is necessary in order to represent the ODF numerically. Equidistant angular steps of Θ and Φ in a polar coordinate system can be used in principle but are rather ineffective. Because of the inadequate spatial distribution of the resulting grid points on the surface of the unit sphere using equidistant angular steps, the density of the grid points at the poles is considerably higher than at the equatorial plane. Accordingly, depending on the choice of the angular steps, both the computational effort is too high and/or the resolution at the equatorial plane is too low.

Weber et al. used an improved formulation of the unit sphere using equidistant angular steps in the pole direction and azimuth angular steps as a function of the pole angle. This results in a surface grid with almost identical surface areas [31]. However, the shapes of the surface areas are very different at the equatorial plane and the poles.

Another simple method to create a unit sphere with approximately the same density of grid points is to create an icosphere. The starting point of this method is a regular icosahedron, which is represented by the following 12 points:

$$\begin{array}{l} (-1 \quad t \quad 0) \\ (1 \quad t \quad 0) \\ (-1 \quad -t \quad 0) \\ (1 \quad -t \quad 0) \end{array} \quad \begin{array}{l} (0 \quad -1 \quad t) \\ (0 \quad 1 \quad t) \\ (0 \quad -1 \quad -t) \\ (0 \quad 1 \quad -t) \end{array} \quad \begin{array}{l} (t \quad 0 \quad -1) \\ (t \quad 0 \quad 1) \\ (-t \quad 0 \quad -1) \\ (-t \quad 0 \quad 1) \end{array}$$

with $t = \frac{1+\sqrt{5}}{2}$. The convex hull of the point cloud is the regular icosahedron. The convex hull consists of 20 triangles of equal size. To refine the regular icosahedron to the icosphere, each of the triangles is divided into 4 smaller triangles. For this purpose, the center of each edge of the triangles is calculated and projected onto the surface of the unit sphere. This procedure can be repeated as often as needed. In this paper, the center points of the surfaces were used as grid points for the evaluation of ψ . Therefore, the number of grid points n_{grid} is equal to the number of triangles. Figure 3 shows the evolution of the icosphere with increasing refinement level ref . A refinement level of $ref = 5$ with a total of 20,480 grid points was used entirely in this work.

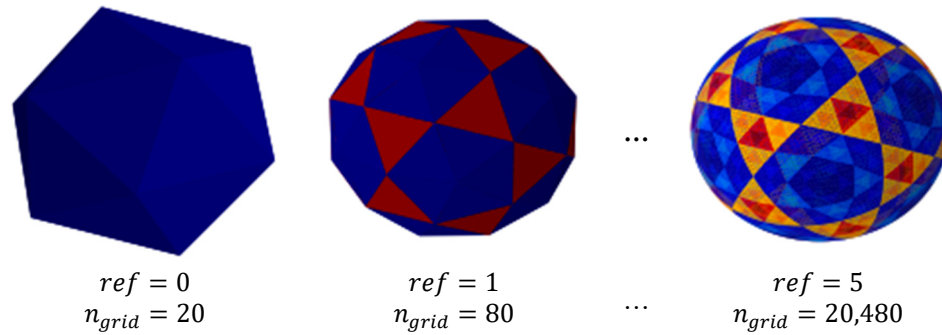


Figure 3. Evolution of icosphere with refinement level 0, 1, and 5. The color represents the relative area of the triangles.

4. Reconstruction Methods

The two reconstruction methods considered in this contribution are described shortly in the following section. They are, on the one hand, the spherical harmonics and, on the other hand, the method of maximum entropy.

4.1. Spherical Harmonics

Spherical harmonics is based on the description of fiber orientation as a Laplace series or a generalized Fourier series [2]. Each twice-integrable function can be represented on the unit sphere

surface as a series representation of tensors. The series can be carried out up to order N . Due to the symmetry of $\psi(\mathbf{p})$, only even-order tensors are used here. In the following, the equations for the reconstruction $\hat{\psi}_N$ by spherical harmonics are listed, and a general derivation of the equation can be found in [2,32]. The reconstruction of the fiber orientation is determined by the sum of the moments:

$$\hat{\psi}_N(\Theta, \Phi) = \sum_{l=0}^N \alpha_l(\Theta, \Phi). \quad (13)$$

The general definition for the moments $\alpha_l(\mathbf{p})$ is:

$$\alpha_l(\Theta, \Phi) = \sum_{m=0}^l \beta_l^m(\Theta, \Phi), \quad (14)$$

with:

$$\begin{aligned} \beta_l^m(\Theta, \Phi) = & \left(1 - \frac{1}{2} \delta_{m0} \right) \left(\frac{1}{\pi} P_l^m(\cos \Theta) \cos(m\Phi) \oint_{\mathbb{S}} \psi(\Theta, \Phi) P_l^m(\cos \Theta) \cos(m\Phi) d\mathbb{S} \right. \\ & \left. + \frac{1}{\pi} P_l^m(\cos \Theta) \sin(m\Phi) \oint_{\mathbb{S}} \psi(\Theta, \Phi) P_l^m(\cos \Theta) \sin(m\Phi) d\mathbb{S} \right), \end{aligned} \quad (15)$$

and:

$$P_l^m(\mu) = (-1)^m \sqrt{\frac{2l+1}{2} \frac{(l-m)!}{(l+m)!} \frac{1}{2^l \cdot l!} (1-\mu^2)^{\frac{m}{2}} \frac{d^{m+l} (\mu^2 - 1)^l}{d\mu^{m+l}}}. \quad (16)$$

The integrals occurring in Equation (15) for the calculation of $\beta_l^m(\Theta, \Phi)$ are replaced by the corresponding entries of the fiber orientation tensors of Equation (9).

4.2. Method of Maximum Entropy

Mathematically, the problem of the reconstruction of an ODF based on fiber orientation tensors is ill-posed, since there is no unique solution (see Figure 2). One way to find a unique solution to an ill-posed problem is to use the maximum entropy method. This method provides the solution that is coherent with the known information and has the highest entropy. The maximum entropy approach can be successfully applied to many ill-posed problems, such as spectral analysis or image restoration [33]. In the framework of the reconstruction of orientation tensors in order to consider anisotropic mechanical properties of short-fiber reinforced plastics, the maximum entropy approach is already applied in commercial software [34]. A summary and overview of the maximum entropy method is provided by Wu [33].

In the context of fiber orientation, entropy is the deviation of the ODF. Analogous to Shannon's definition in [35] the mathematically definition of the entropy is:

$$S = - \oint_{\mathbb{S}} \psi \ln \psi d\mathbb{S}. \quad (17)$$

Therefore, a unidirectional fiber distribution has an entropy of $S = 0$. Applying the maximum entropy method to the reconstruction problem results with the finding of the ODF that has a maximum scatter of the orientation distribution function for a given fiber orientation tensor. This idea is supported by the findings of Hine et al. [36]. They confirmed on the basis of experimental measurements that real microstructures of injection molded or extruded samples exhibit a maximum entropy of fiber orientation. In addition, Müller [37] showed already in his work that if real microstructures show a fiber orientation with maximum scattering of fiber distribution function, the method of maximum entropy method is suitable for determining the linear elastic composite properties.

The distribution function reconstructed in this investigation is a Bingham distribution, which corresponds to a normal distribution on the unit sphere surface [38]. The Bingham distribution is accordingly π -periodic. In principle, other distribution functions could also be used with this method. A bivariate Bingham distribution is defined with [39]:

$$f(\bar{x}) = e^{-\alpha\bar{x}_1^2 + \beta\bar{x}_3^2}. \quad (18)$$

To create a Bingham distribution, the expected value μ and the covariance $\Sigma = (\alpha, \beta)$ is required. The modification of the Bingham distribution is done by formulating a minimization problem. In the context of this investigation, the second-order fiber orientation tensor is used for the minimization problem. This means that the Bingham distribution is modified in such a way that the second-order fiber orientation tensor calculated of the modified distribution corresponds to the given second-order fiber orientation tensor. The minimization problem of the reconstruction with the maximum entropy method is defined by:

$$f(x) = (d_{ix}w_i - a_{xx})^2 + (d_{iy}w_i - a_{yy})^2 + (d_{iz}w_i - a_{zz})^2, \quad (19)$$

with the constraint:

$$\sum_i w_i - 1 = 0. \quad (20)$$

Here, w_i is the probability with which a fiber points in the corresponding direction \bar{p}_i . This direction is the normal direction of the icosphere–triangle with the index i . The probability is calculated by the Bingham distribution given by:

$$w_i = J_i e^{(x_j d_{ij} + x_4)}. \quad (21)$$

J_i is the area of the icosphere–triangle, and x_1 to x_4 are the coefficients of the Bingham distribution. Furthermore, there is:

$$d_{ij} = \bar{p}_{ij}^2, \quad (22)$$

with \bar{p}_{ij} as the components of the midpoint of the icosphere–triangle, which is rotated into the principal axis of the expected value. The rotation can be performed with a scalar product of a corresponding rotation matrix R :

$$\bar{p} = R \cdot p. \quad (23)$$

The minimization problem can be solved by any suitable numerical method if it is able to fulfill the constraint. One such method is sequential least square programming (SLSQP) [40]. In addition, it was examined whether the constraint can be replaced by a simple normalization of $\hat{\psi}$ at the end of the numerical minimization. This would have the advantage that faster numerical methods can be used. Here, the conjugate gradient (CG) algorithm of Polak and Ribiere was applied [41]. Within the framework of this work, both numerical methods were carried out to an accuracy of the result of 10^{-18} . This means that the abort criterion of the numerical methods is satisfied if $f(x)$ is smaller than the required accuracy.

5. Evaluation

The reconstruction methods were evaluated by comparing the results in terms of accuracy and computational effort. The basis for the investigation was provided by various test scenarios, whose creation is explained in more detail in the following section. One test scenario is an explicitly given initial ODF. This initial ODF was used to estimate the fiber orientation tensors, which were used as inputs for the reconstruction methods. With this approach, it is possible to compare the reconstructed ODFs against each other as well as against the initial ODF. Both the accuracy of the reconstruction and the numerical effort, measured by the required computing time, were compared. The spectral decomposition was repeated for the steps $l = 2$ to $l = 8$. In addition, the higher-order tensors were calculated once from the initial ODF and once by closures from the lower-order tensors.

Table 4 gives an overview of the reconstruction methods used and their variants. The fiber orientation tensors used for the reconstruction are indicated. In the following, the methods are only indicated by their abbreviations. ME stands for maximum entropy and SH for spherical harmonics. The number after SH indicates the maximum order N used for the reconstruction. The abbreviation HY at the end stands for the use of the hybrid closure of the highest tensor, and HYHY for the consecutive use of the hybrid closure.

Table 4. List of used reconstruction methods and their input.

Method	Abbreviation	$\hat{\psi}$	a_2	a_4	a_6	a_8
Method of Maximum Entropy	ME	$f(a_2)$	$f(\psi)$			
Spherical Harmonics (2nd order)	SH2	$f(a_2)$	$f(\psi)$			
Spherical Harmonics (4th order)	SH4	$f(a_2, a_4)$	$f(\psi)$	$f(\psi)$		
Spherical Harmonics (6th order)	SH6	$f(a_2, a_4, a_6)$	$f(\psi)$	$f(\psi)$	$f(\psi)$	
Spherical Harmonics (8th order)	SH8	$f(a_2, a_4, a_6, a_8)$	$f(\psi)$	$f(\psi)$	$f(\psi)$	$f(\psi)$
Spherical Harmonics (4th order, with hybrid closure)	SH4HY	$f(a_2, \hat{a}_4)$	$f(\psi)$	$\hat{a}_4 = f(a_2)$ Hybrid Closure		
Spherical Harmonics (6th order, with hybrid closure)	SH6HY	$f(a_2, a_4, \hat{a}_6)$	$f(\psi)$	$f(\psi)$	$\hat{a}_6 = f(a_2, \hat{a}_4)$ Hybrid Closure	
Spherical Harmonics (6th order, with hybrid closure for 4th and 6th order tensor)	SH6HYHY	$f(a_2, \hat{a}_4, \hat{a}_6)$	$f(\psi)$	$\hat{a}_4 = f(a_2)$ Hybrid Closure	$\hat{a}_6 = f(a_2, \hat{a}_4)$ Hybrid Closure	

5.1. Tests Scenarios

Two different test variants of the test scenarios were considered. On the one hand, a fiber orientation was created on the basis of a Bingham distribution and, on the other hand, measured fiber orientation from the literature was used.

The idea of fiber orientation with a Bingham distribution is based on the solution of the Fokker–Plank equation. Chaubal and Leal limited the flow conditions at which a Bingham distribution of the Fokker–Planck equation can be expected [13]. To create a Bingham distribution, the expected value μ and the covariance Σ are required. The expected value specifies the position of the maximum of the distribution. The covariance, on the other hand, determines the scattering width of the distribution. The expected value μ was exemplarily chosen to be on the equatorial plane with $\mu = \frac{1}{2}(\pi, \pi)$. The covariance was varied in order to create the different test scenarios. The variation was chosen in such a way that the fiber orientation corresponds to unidirectional, orthotropic with respect to the equatorial and meridian plane, and quasi-isotropic conditions. For this purpose, α and β (see Equation (17)) were independently varied in 20 logarithmically equidistant steps from 10^{-4} to 10^4 resulting in a total of 400 individual test scenarios.

5.2. Evaluation Criteria

For the complete evaluation of the reconstruction methods, a measure of the similarity of two probability distributions P and Q is required. For that, the sum of the squared errors between initial and computed ODF can be considered by:

$$E^2 = \int_{-\infty}^{\infty} (P - Q)^2. \quad (24)$$

A further measure for evaluation is the Kullback–Leibner distance [42]:

$$D_2(P \parallel Q) = D(P \parallel Q) + D(Q \parallel P), \quad (25)$$

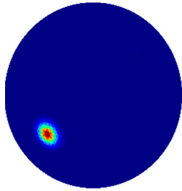
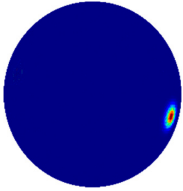
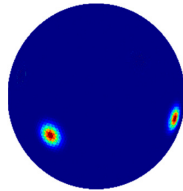
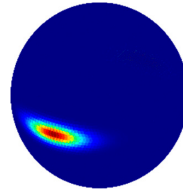
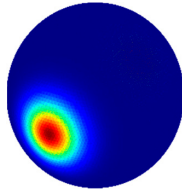
which can be calculated by the Kullback–Leibner divergence:

$$D(P \parallel Q) = \int_{-\infty}^{\infty} p(x) \cdot \log \frac{p(x)}{q(x)} dx. \quad (26)$$

A Kullback–Leibner distance of $D(P \parallel Q) = 0$ means that both probability distributions are identical. However, the greater the value of the Kullback–Leibner distance is, the more different the probability distributions are.

Some examples of comparisons between ODFs should illustrate the difference of the evaluation criteria. Table 5 shows a total of 5 ODFs. Each of the 5 ODFs is compared with the first ODF ψ_0 , and the evaluation criteria are determined. This shows that the integral error E is by definition largest if the expected value is not identical (ψ_1) and the distributions do not overlap. The Kullback–Leibner distance in this case is 0 because the distribution is the same. The Kullback–Leibner distance, on the other hand, is largest in the case of ψ_4 . Thus, the Kullback–Leibner distance gives a more useful estimation with regard to the shape of the ODF.

Table 5. Comparison of ODFs (with ψ_0) for the illustration of evaluation criteria.

ψ_0 (Reference)	ψ_1	ψ_2	ψ_3	ψ_4
				
$D = 0.0$ $E = 0.0$	$D = 0.0$ $E = 0.159$	$D = 0.346$ $E = 0.079$	$D = 2.767$ $E = 0.081$	$D = 4.461$ $E = 0.112$

5.3. Numerical Results for Bingham Distributions

First, some selected test scenarios were evaluated in order to demonstrate the principal differences between the reconstruction methods. A total of five different test scenarios are presented as examples. Each of these five test scenarios represents a qualitatively different challenge for the reconstruction methods. The test scenarios include two unidirectional fiber orientations, the first with nearly perfect orientation and the second with a somewhat more scattered fiber alignment. Furthermore, two fiber orientations with different scattering widths in azimuth and polar directions were selected. Finally, a planar-isotropic fiber orientation was chosen. In the following figures for the individual test scenarios, the probability of a fiber pointing in one direction is represented by color: A value of 0 corresponds to the color blue, while the maximum value is always colored red.

The first test scenario of a unidirectional distribution is shown in Figure 4 in combination with its reconstructions. It is easy to recognize that the ME method reconstructs an ODF that is almost identical to the initial ODF. The methods SH2 to SH8, on the other hand, reconstruct an ODF with a much broader distribution and a less pronounced secondary maximum. The broader distribution is due to the used moments, which are unsuitable to approximate a unidirectional fiber distribution. The reconstruction using the closures does not provide any further information, since the hybrid closure is exact for unidirectional distributions. Thus, the reconstructions SH4HY, SH6HY, and SH6HYHY are identical to SH4 and SH6, respectively.

The next test scenario is given in Figure 5 with a distribution that is similar to the first test scenario, but with a broader scattering width. The reconstruction using ME provides again an almost identical ODF compared with the initial ODF. The reconstructions SH2 and SH4 show again a larger scattering than the initial ODF. Only for SH6 and SH8 are the moments sufficient to reproduce the distribution close enough. Like in the first test scenario, secondary maxima are also recognizable by all spherical harmonic reconstructions except SH2. The SH4HY and SH6HY reconstructions are very similar to

the SH4 and SH6 reconstructions, as the hybrid closure is performing well in this case. By contrast, the reconstruction SH6HYHY differs strongly from the test scenario. Both the scattering range and the secondary maximum are much more pronounced. In addition, the expected value is distributed symmetrically to two points in relation to the expected value of the test scenario. The consecutive application of hybrid closure is therefore not suitable in this case.

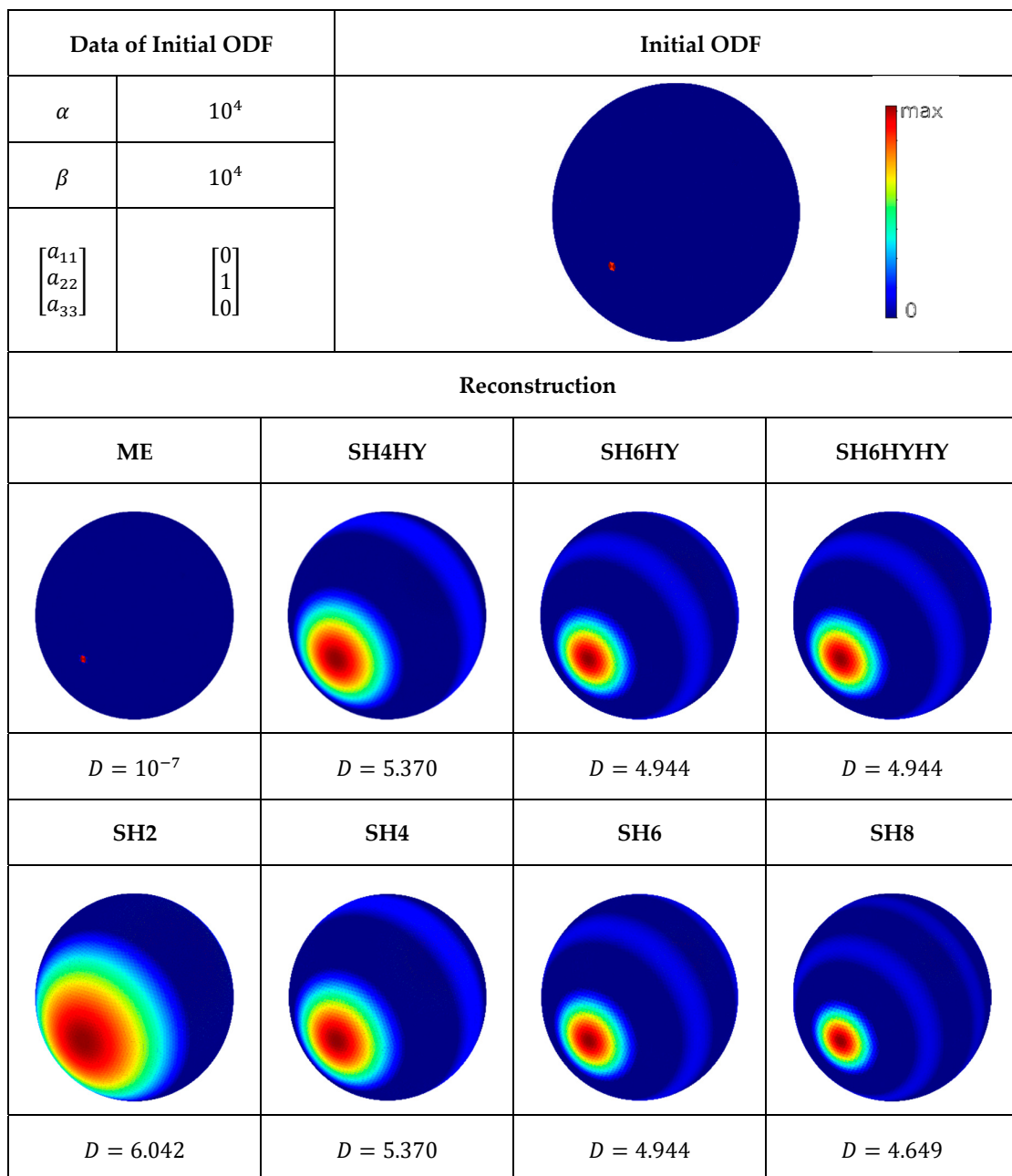


Figure 4. Top: Initial ODF and data of first test case. Bottom: Reconstruction of test case with the different reconstruction methods.

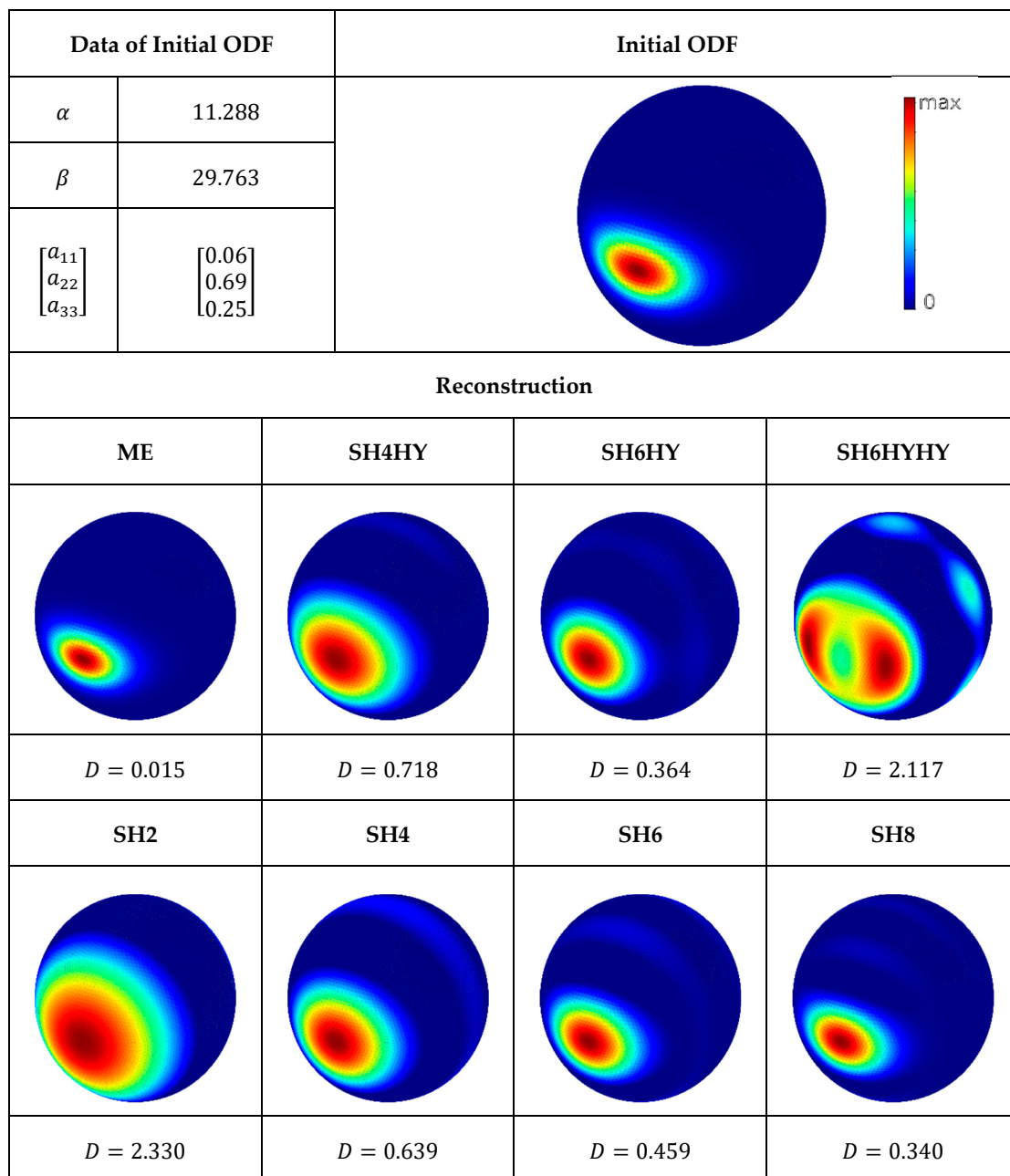


Figure 5. Top: Initial ODF and data of second test case. Bottom: Reconstruction of test case with the different reconstruction methods.

Figure 6 represents the next test scenario in comparison to the corresponding reconstructions. The ODF of this test scenario is characterized by a sharply limited distribution in the meridian plane, where the value at the pole positions is zero. The ME again provides the best reconstruction, where only the values of the ODF from pole to equator are slightly different. The sharp definition of the initial ODF at the poles of this test scenario is reconstructed more diffusely. The reconstructions SH2 to SH8 deliver, as expected, a too-broad ODF due to the too-few moments of spectral approximation. The secondary maxima are more pronounced in this test scenario than in the previous ones. In this test scenario, the effect of using the hybrid closure to calculate the higher tensors is particularly interesting. The reconstruction SH4HY shows two equal maxima, which are symmetrically arranged to the equatorial plane. Nevertheless, the Kullback–Leibner distance with $D = 3.150$ is approximately equal to the Kullback–Leibner distance of the reconstruction SH4. The reconstruction SH4HY illustrates

the problems of using closures. Assumptions or, generally speaking, the applicability of a closure, cannot be supposed to be true in a reconstruction problem, since no information about the original ODF is known. Accordingly, the use of closures can be doubtful for the reconstruction, although higher moments are used which should be beneficial for sharply limited ODFs.

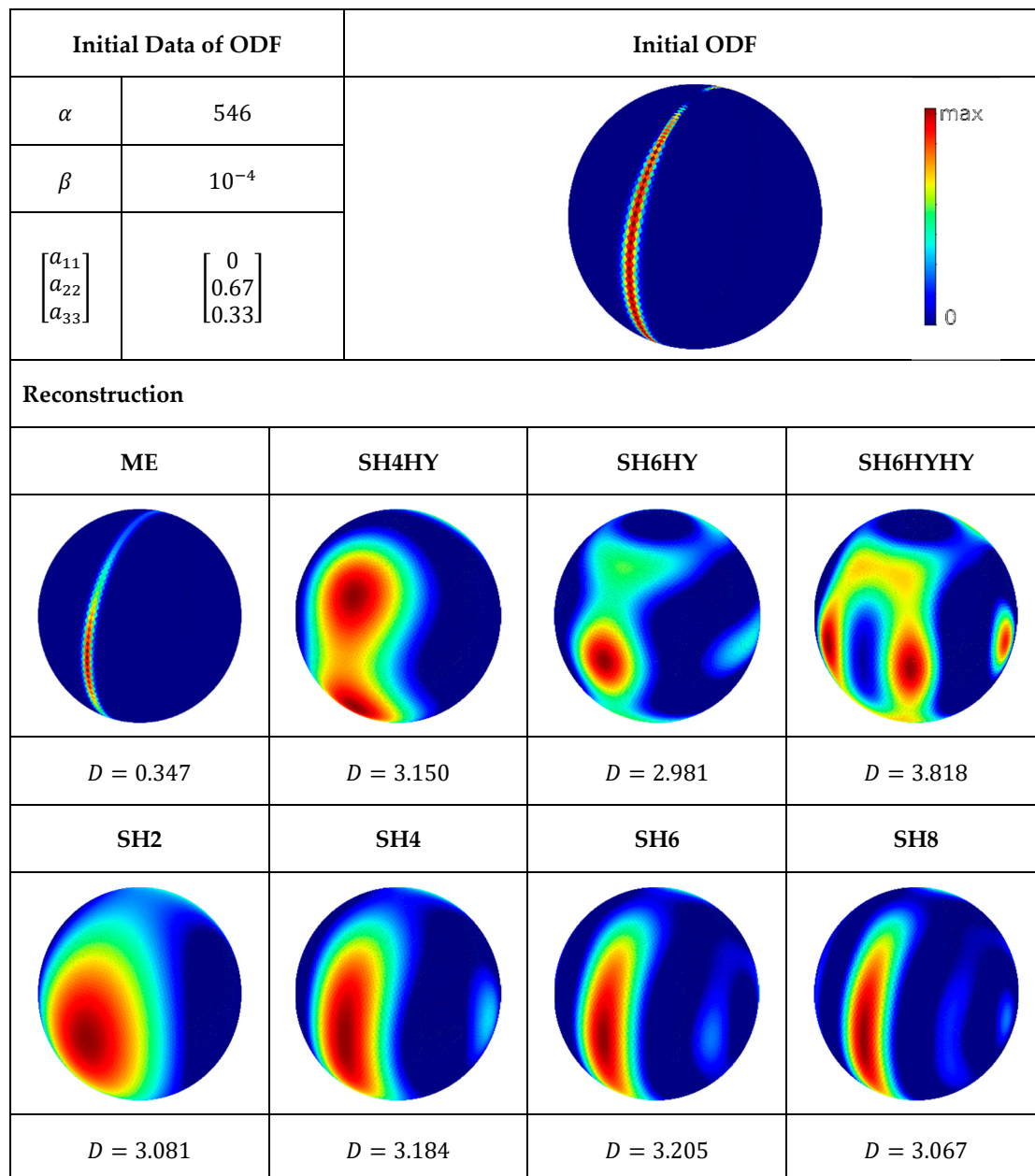


Figure 6. Top: Initial ODF and data of third test case. Bottom: Reconstruction of test case with the different reconstruction methods.

The fourth test scenario is shown in Figure 7. The distribution is relatively broad in the meridian plane as well as over the circumference. At the poles, however, an extremely sharp border results from the fact that the even distribution on the meridian planes is diminishing as they are getting closer to each other. In contrast to the previous test procedures, the ME method appears not to be the best solution, as it does not provide sharp distribution at the poles. In the reconstructions SH4 to SH8, several maxima can be observed, which merge more and more together as the number of moments increases.

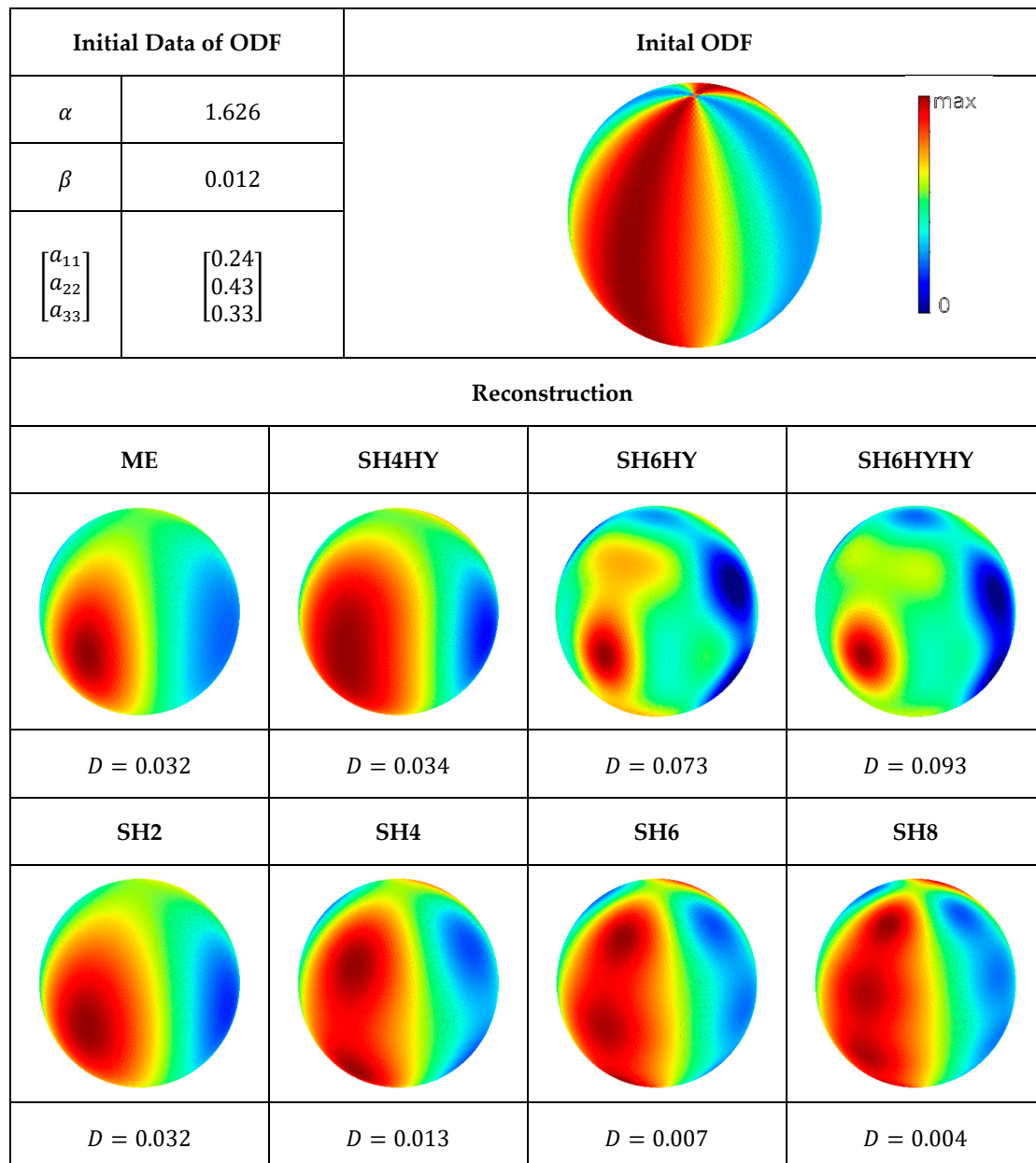


Figure 7. Top: Initial ODF and data of fourth test case. Bottom: Reconstruction of test case with the different reconstruction methods.

The last example of test scenarios shows a relatively broad, almost circumferential distribution on the equatorial plane (see Figure 8). The reconstruction using ME is exact. Once again, the reconstruction using hybrid closure is questionable. Several maxima occur in the reconstructions SH4HY, SH6HY, and SH6HYHY and are much more pronounced than in the previous test scenarios. Furthermore, the Kullback–Leibner distance is significantly worse compared to the reconstructions SH4 and SH6.

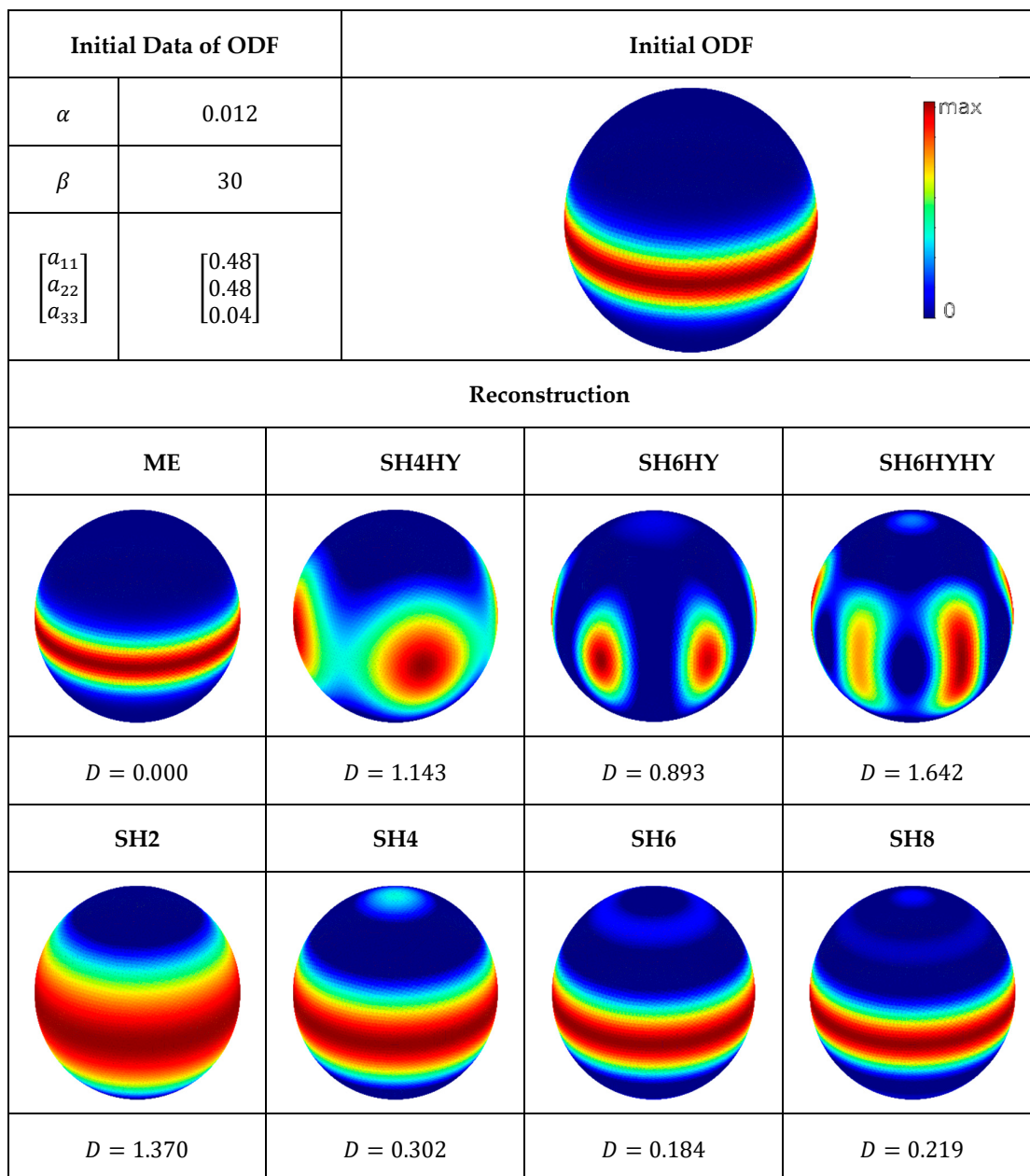


Figure 8. Initial ODF and data of fifth test case. Bottom: Reconstruction of test case with the different reconstruction methods.

In the following, all test scenarios for the evaluation of the reconstruction methods are compared against each other. First, the methods SH2 to SH8 are analyzed. The Kullback–Leibner distance as a function of the logarithmically covariances φ and θ is shown in Figure 9. The value of the Kullback–Leibner distance is represented by a color. The figure shows that the reconstruction methods SH2 to SH8 are qualitatively very similar. In the range of nearly unidirectional initial fiber orientation, the Kullback–Leibner distance is large, whereas in the range of isotropic initial fiber orientation, the Kullback–Leibner distance is nearly zero. As the number of moments increases, the Kullback–Leibner distance becomes smaller, but still not significant.

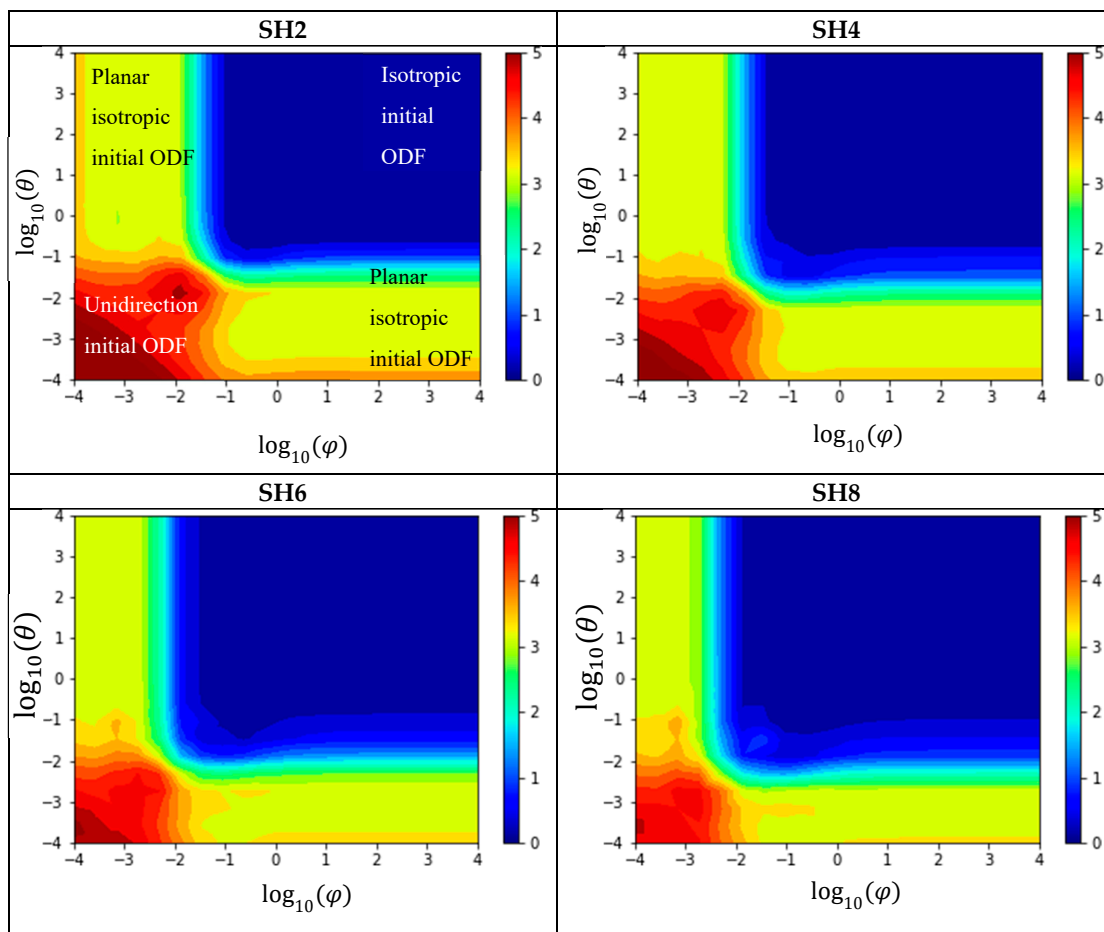


Figure 9. Color plot of the Kullback–Leibner distance in dependency of covariance (SH2, SH4, SH6, and SH8).

The reconstructions SH4HY, SH6HY, and SH6HYHY, shown in Figure 10, differ essentially from SH4 and SH6 in cases where one of the covariances is small and the other large. In these cases, the Kullback–Leibner distance is either greater or smaller. Especially in SH6HYHY reconstructions, both cases occur simultaneously. The evaluation of the Kullback–Leibner distance in SH4HY, SH6HY, and SH6HYHY is no longer symmetrical to the bisector. An exact explanation of the differences with hybrid closure is therefore accordingly difficult. It is known that the hybrid closure overestimates the fiber alignment. This is counteracted by a too-low order of moment used. The shown comparison is designed in such a way that the methods SH2 to SH8 get the exact tensors of higher order and should therefore have a lower Kullback–Leibner distance. The supposed improvement of the Kullback–Leibner distance using the hybrid closure is therefore not to be regarded as an improvement as such, but rather as more or less random, as the overprediction of alignment equalizes the too-low order of moments.

The reconstruction with ME shows a consistently low Kullback–Leibner distance. This proves that the maximum entropy method is capable of reconstructing a distribution function so far as all information is contained in the fiber orientation tensor. This is the case in the example of the Bingham distribution chosen here, since the expected value is clearly determined by the eigenvectors of the second-order fiber orientation tensor, and the scatter can be determined from the eigenvalues.

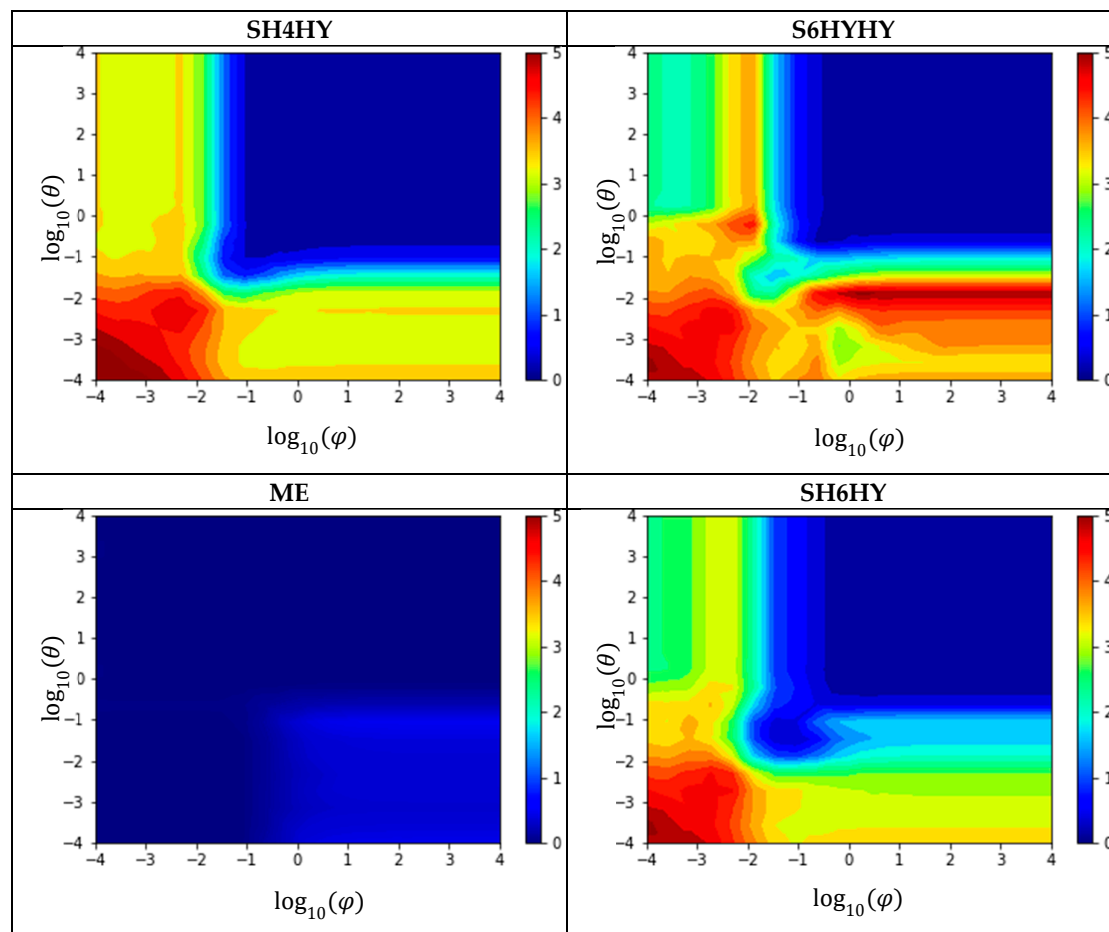


Figure 10. Color plot of the Kullback–Leibner distance in dependency of covariance (SH4HY, SH6HY, SH6HYHY, and ME).

In the context of a reconstruction problem, the quality of the reconstruction as well as the computing time is of interest. Figure 11 shows the time required to perform a reconstruction. The indicated time refers exclusively to the reconstruction, i.e., the calculation of the fiber orientation tensors of the initial ODF is not considered. The performed benchmark is implemented in the programming language Python, whereby each reconstruction method is vectorized and sped up as far as possible. The benchmark is performed on an AMD Ryzen 7 1800X system (Advanced Micro Devices, Inc., Santa Clara, CA, USA). As already mentioned, the influence of the numerical method of the ME method on the required computing time is analyzed. Note that due to the specified tolerance, the reconstruction is identical for both numerical methods.

In Figure 11, the time is given relative to ME SLQP, which on average takes 1.29 s. It turns out that the SH2 method is the fastest. SH4 to SH8 are about 30% slower, although interestingly, there is no significant difference between SH4, SH6, and SH8. The ME method with the CG algorithm is about 65% slower than the SH2 method. With the SLSQP algorithm, the ME method is considerably slower than with the CG algorithm.

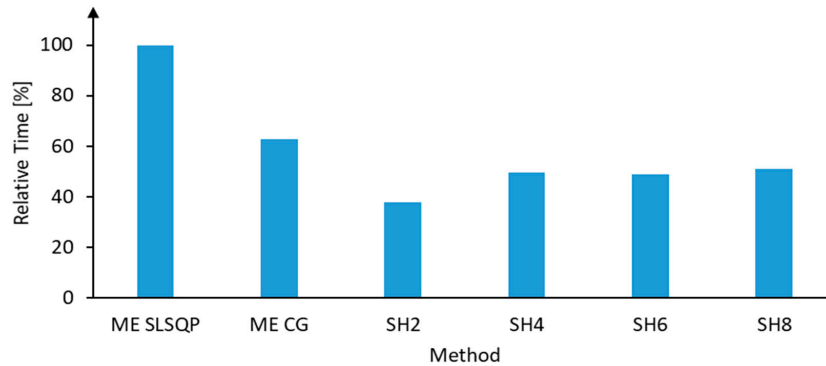


Figure 11. Overview of average computational time of the reconstruction methods.

5.4. Numerical Results for Measured Data

In addition to the synthetic benchmarks in Section 5.3, measured fiber orientation was used for comparison. These data originate exclusively from the literature.

The first set of data was taken from [7] and is shown in Figure 12 together with the reconstructions. The methods SH2 to SH8 can reconstruct the data relatively well, whereby the absolute height at the expected value is clearly underestimated, especially for SH2 and SH4. The scatter of the reconstructions is wider than the original ODF. The reason for that was already discussed for the Bingham test scenarios: The number of moments used is too low to be able to represent the peak. The reconstructions based on the hybrid closure again show a completely different behavior. Several maximum values are reconstructed, as well as a shift of the expected value. The ME method reconstructs the ODF relatively well, although with a too-low probability density around the maximum of the initial ODF and a too-wide scattering, especially at -30° and $+50^\circ$.

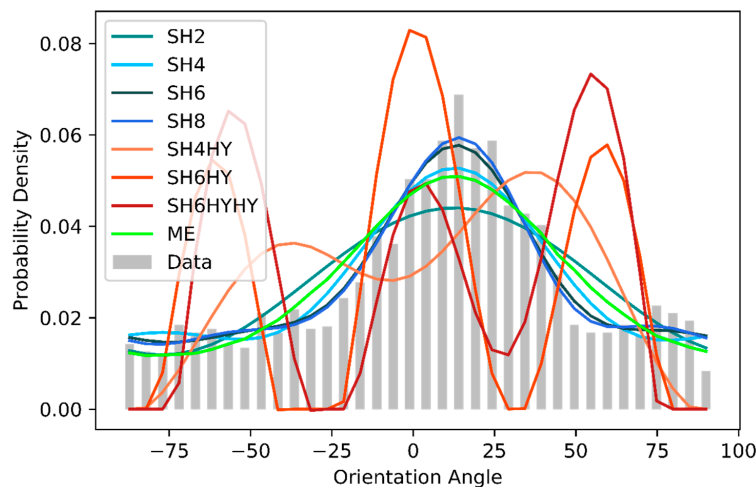


Figure 12. Measured and reconstructed ODFs from [7].

The second set of data was taken from [43]. The fiber orientation was measured by μ Computer Tomography (μ CT) of injection molded samples. Subsequently, the ODF was subdivided into shell and core layers, with the shell layer used here. In this dataset, the peak at 90° is particularly interesting in respect of to what extent it can be reconstructed (see Figure 13). In the area around the expected value, the behavior is basically similar to that of the first set of data. The methods SH2 to SH8 and ME underestimate the absolute value at the expected value. With SH2 and ME, the reconstructed probability at $\pm 50^\circ$ is again too high, and the peak at 90° cannot be reconstructed. Here, only the methods SH4, SH6, and SH8 can generate something that is similar to a second peak. The reconstruction methods with hybrid closure reconstruct several maxima symmetrically to the expected value again.

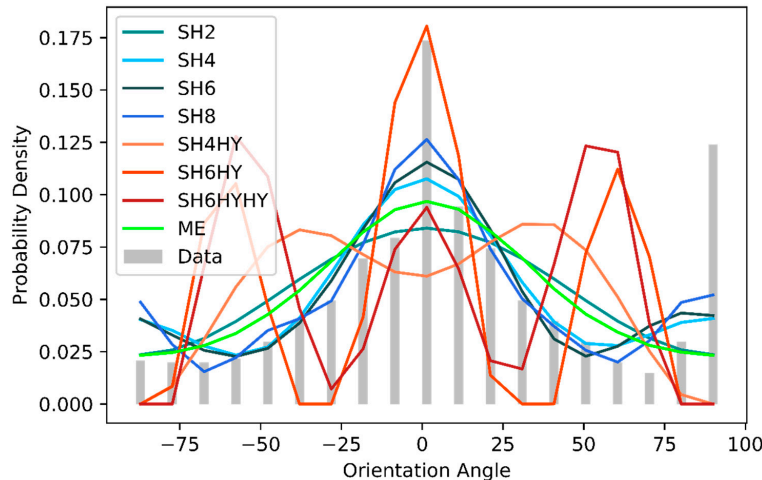


Figure 13. Measured and reconstructed ODFs from [43].

The third ODF was taken out of Lenke [44]. In this case, however, the direct numerical values of the μ CT-experimentally-measured ODF were not used, but a probability density function that represents the measured data in an extremely good approximation. The probability density function is described in Lenke's work by:

$$h(\theta) = \frac{h_2}{\sqrt{1 - \frac{h_1^2 - h_2^2}{h_1^2} \cdot \cos^2(\theta)}}. \quad (27)$$

The reconstruction of the methods is exactly analogous to the previous examples. Figure 14 shows the results. The methods SH2 to SH8 become better with each increasing moment to reconstruct the ODF. Here, an oscillation is very noticeable apart from the expected value. The reconstructions with hybrid closures generate several maxima again. In addition to that, it becomes evident that the ME method does not work well enough here, because the original ODF is not a Bingham distribution.

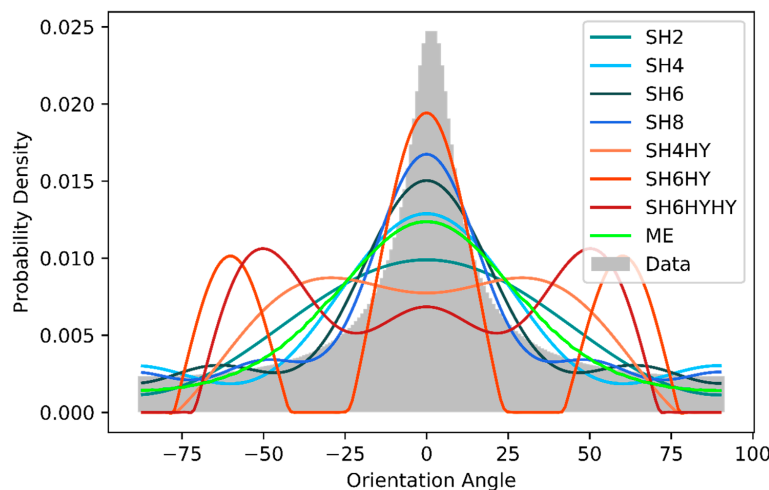


Figure 14. Measured and reconstructed ODFs from [44].

6. Conclusions

The aim of this work was to compare and evaluate existing reconstruction methods of a fiber orientation distribution based on fiber orientation tensors. The evaluation was based on the Kullback–Leibner distance as well as on a direct qualitative comparison of the obtained distributions.

In a first step, initial ODFs were generated and the related fiber orientation tensors were determined. Using reconstruction methods, the approximated ODF was calculated on the basis of the fiber orientation tensors. The initial ODFs generated were of a Bingham distribution type, and experimentally measured data from the literature were also used.

None of the investigated reconstruction methods can be considered as the best in general. Although the maximum entropy method impressively shows that a certain distribution can be reconstructed almost identically, this is only if the distribution type is of the same type. The Bingham distribution chosen in this paper was practically reconstructed one-to-one by the maximum entropy method. In the reconstruction of the measured data, however, the weakness of the maximum entropy method becomes apparent: Distributions different from a Bingham distribution or outliers cannot be reconstructed. This is a strength of the spectral harmonics approximations, which in principle could represent any distribution function. Nevertheless, this reconstruction method cannot be considered ideal either, since the moments in particular must be correspondingly high in order to be able to map certain distribution functions. It has been shown that even with the fiber orientation tensor of the eighth order included, sharply limited distributions cannot be reconstructed. Moreover, these high moments are usually not available in process simulations. Although closures offer the possibility of higher moments, however, the problem here are the closures themselves, since assumptions have to be made about the distribution function.

With the mentioned advantages and disadvantages of both reconstruction methods, it can be concluded that in the case of the reconstruction of an ODF only on the basis of a second-order fiber orientation tensor without any further information about the ODF, the maximum entropy method seems to be on average the best choice. This is evident from the following two reasons: Firstly, the assumption of maximum entropy is a physical approach, which Hine et al. [36] can largely confirm with experimentally measured fiber orientations. Secondly, the reconstructions in this contribution show that the errors of the maximum entropy method are much smaller than those of the frequently used SH4HY method (spherical harmonics, 4th order, with hybrid closure).

Author Contributions: K.B., M.S. and W.K. conceived the investigation. K.B. wrote the software. K.B. and M.S. analyzed the data. K.B. did the visualization. Writing the paper was done by all three authors.

Funding: This research was supported by the German National Science Foundation (DFG) within the Project STO 910/13-1.

Conflicts of Interest: The authors declare no conflict of interest.

References

1. Jeffery, G.B. The Motion of Ellipsoidal Particles Immersed in a Viscous Fluid. *Proc. R. Soc. A Math. Phys. Eng. Sci.* **1922**, *102*, 161–179. [[CrossRef](#)]
2. Jack, D.A. Advanced Analysis of Short Fiber Polymer Composite Material Behavior. Ph.D. Thesis, University of Missouri, Columbia, MO, USA, 2006.
3. Risken, H. *The Fokker-Planck Equation. Methods of Solution and Applications*, 2nd ed.; Springer: Berlin, Germany, 1996; ISBN 978-3-540-61530-9.
4. Einstein, A. Über die von der molekularkinetischen Theorie der Wärme geforderte Bewegung von in ruhenden Flüssigkeiten suspendierten Teilchen. *Ann. Phys.* **2005**, *14*, 182–193. [[CrossRef](#)]
5. Folgar, F.; Tucker, C.L. Orientation Behavior of Fibers in Concentrated Suspensions. *J. Reinf. Plast. Compos.* **1984**, *3*, 98–119. [[CrossRef](#)]
6. Hand, G.L. A theory of anisotropic fluids. *J. Fluid Mech.* **1962**, *13*, 33–46. [[CrossRef](#)]
7. Advani, S.G.; Tucker, C.L. The Use of Tensors to Describe and Predict Fiber Orientation in Short Fiber Composites. *J. Rheol.* **1987**, *31*, 751–784. [[CrossRef](#)]
8. Doi, M. Molecular dynamics and rheological properties of concentrated solutions of rodlike polymers in isotropic and liquid crystalline phases. *J. Polym. Sci. Polym. Phys. Ed.* **1981**, *19*, 229–243. [[CrossRef](#)]
9. Marrucci, G.; Grizzuti, N. Predicted effect of polydispersity on rodlike polymer behaviour in concentrated solutions. *J. Non-Newton. Fluid Mech.* **1984**, *14*, 103–119. [[CrossRef](#)]

10. Agboola, B.O.; Jack, D.A.; Montgomery-Smith, S. Effectiveness of recent fiber-interaction diffusion models for orientation and the part stiffness predictions in injection molded short-fiber reinforced composites. *Compos. Part A Appl. Sci. Manuf.* **2012**, *43*, 1959–1970. [[CrossRef](#)]
11. Montgomery-Smith, S.; He, W.; Jack, D.A.; Smith, D.E. Exact tensor closures for the three-dimensional Jeffery's equation. *J. Fluid Mech.* **2011**, *680*, 321–335. [[CrossRef](#)]
12. Montgomery-Smith, S.; Jack, D.; Smith, D.E. The Fast Exact Closure for Jeffery's equation with diffusion. *J. Non-Newton. Fluid Mech.* **2011**, *166*, 343–353. [[CrossRef](#)]
13. Chaubal, C.V.; Leal, L. A closure approximation for liquid-crystalline polymer models based on parametric density estimation. *J. Rheol.* **1998**, *42*. [[CrossRef](#)]
14. Cintra, J.S.; Tucker, C.L. Orthotropic closure approximations for flow-induced fiber orientation. *J. Rheol.* **1995**, *39*, 1095–1122. [[CrossRef](#)]
15. De Frahan, H.H.; Verleye, V.; Dupret, F.; Crochet, M.J. Numerical prediction of fiber orientation in injection molding. *Polym. Eng. Sci.* **1992**, *32*, 254–266. [[CrossRef](#)]
16. Jack, D.A.; Schache, B.; Smith, D.E. Neural network-based closure for modeling short-fiber suspensions. *Polym. Compos.* **2010**, *31*, 1125–1141. [[CrossRef](#)]
17. Qadir, N.U.; Jack, D.A. Modeling fibre orientation in short fibre suspensions using the neural network-based orthotropic closure. *Compos. Part A Appl. Sci. Manuf.* **2009**, *40*, 1524–1533. [[CrossRef](#)]
18. Feng, J.; Chaubal, C.V.; Leal, L.G. Closure approximations for the Doi theory: Which to use in simulating complex flows of liquid-crystalline polymers? *J. Rheol.* **1998**, *42*, 1095–1119. [[CrossRef](#)]
19. Hinch, E.J.; Leal, L.G. Constitutive equations in suspension mechanics. Part 2. Approximate forms for a suspension of rigid particles affected by Brownian rotations. *J. Fluid Mech.* **1976**, *6*, 187–208. [[CrossRef](#)]
20. Chung, D.H.; Kwon, T.H. Invariant-based optimal fitting closure approximation for the numerical prediction of flow-induced fiber orientation. *J. Rheol.* **2002**, *46*, 169–194. [[CrossRef](#)]
21. Altan, M.C.; Subbiah, S.; Güçeri, S.I.; Pipes, R.B. Numerical prediction of three-dimensional fiber orientation in Hele-Shaw flows. *Polym. Eng. Sci.* **1990**, *30*, 848–859. [[CrossRef](#)]
22. Jack, D.A.; Smith, D.E. An invariant based fitted closure of the sixth-order orientation tensor for modeling short-fiber suspensions. *J. Rheol.* **2005**, *49*, 1091–1115. [[CrossRef](#)]
23. Moldex3D. Fiber Function Overview. Available online: http://support.moldex3d.com/r15/en/sync/sync-for-nx/functionoverview_1.html (accessed on 15 January 2019).
24. Autodesk Simulation. Moldflow's Fiber Orientation Models (Theory). Available online: <http://help.autodesk.com/view/MFIWS/2014/ENU/?guid=GUID-6B3A7386-DE57-450E-BF94-B10BD629EC9B> (accessed on 15 January 2019).
25. Li, T.; Luyé, J.F. Optimization of Fiber Orientation Model Parameters in the Presence of Flow-Fiber Coupling. *J. Compos. Sci.* **2018**, *2*, 73. [[CrossRef](#)]
26. Han, J.H.; Khawaja, A.; Kilic, M.H.; Ingram, K. Identification of fiber orientation prediction error by moldflow on compression molded discontinuous long fiber composites using computed tomography x-ray. In Proceedings of the CAMX 2015—Composites and Advanced Materials Expo, Beijing, China, 27–29 October 2015.
27. Férec, J.; Heniche, M.; Heuzey, M.C.; Ausias, G.; Carreau, P.J. Numerical solution of the Fokker–Planck equation for fiber suspensions: Application to the Folgar–Tucker–Lipscomb model. *J. Non-Newton. Fluid Mech.* **2008**, *155*, 20–29. [[CrossRef](#)]
28. Russell, T.; Heller, B.; Jack, D.A.; Smith, D.E. Prediction of the Fiber Orientation State and the Resulting Structural and Thermal Properties of Fiber Reinforced Additive Manufactured Composites Fabricated Using the Big Area Additive Manufacturing Process. *J. Compos. Sci.* **2018**, *2*, 26. [[CrossRef](#)]
29. Friebel, C.; Doghri, I.; Legat, V. General mean-field homogenization schemes for viscoelastic composites containing multiple phases of coated inclusions. *Int. J. Solids Struct.* **2006**, *43*, 2513–2541. [[CrossRef](#)]
30. Müller, V.; Böhlke, T. Prediction of effective elastic properties of fiber reinforced composites using fiber orientation tensors. *Compos. Sci. Technol.* **2016**, *130*, 36–45. [[CrossRef](#)]
31. Weber, B.; Kenmeugne, B.; Clement, J.C.; Robert, J.L. Improvements of multiaxial fatigue criteria computation for a strong reduction of calculation duration. *Comput. Mater. Sci.* **1999**, *15*, 381–399. [[CrossRef](#)]
32. Jack, D.A.; Smith, D.E. Elastic Properties of Short-fiber Polymer Composites, Derivation and Demonstration of Analytical Forms for Expectation and Variance from Orientation Tensors. *J. Compos. Mater.* **2008**, *42*, 277–308. [[CrossRef](#)]

33. Huang, T.S.; Kohonen, T.; Schroeder, M.R.; Lotsch, H.K.V.; Wu, N. *The Maximum Entropy Method*; Springer: Berlin, Germany, 1997; ISBN 978-3-642-64484-9.
34. PART Engineering GmbH. CONVERSE Documentation V 4.0.6; PART Engineering GmbH: Bergisch Gladbach, Germany, 2019.
35. Shannon, C.E. A mathematical theory of communication. *Bell Syst. Tech. J.* **1948**, *27*, 379–423. [[CrossRef](#)]
36. Hine, P.J.; Lusti, H.R.; Gusev, A.A. On the possibility of reduced variable predictions for the thermoelastic properties of short fibre composites. *Compos. Sci. Technol.* **2004**, *64*, 1081–1088. [[CrossRef](#)]
37. Müller, V. Micromechanical Modeling of Short-Fiber Reinforced Composites. Ph.D. Thesis, Karlsruher Institut für Technologie (KIT), Karlsruhe, Germany, 2016.
38. Breitenberger, E. Analogues of the normal distribution on the circle and the sphere*. *Biometrika* **1963**, *50*, 81–88. [[CrossRef](#)]
39. Bingham, C. An Antipodally Symmetric Distribution on the Sphere. *Ann. Stat.* **1974**, *2*, 1201–1225. [[CrossRef](#)]
40. Kraft, D. A software package for sequential quadratic programming. In *Forschungsbericht-Deutsche Forschungs-und Versuchsanstalt für Luft- und Raumfahrt (DFVLR)*; Royal Society of Chemistry: Cambridge, UK, 1988.
41. Nocedal, J.; Wright, S.J. *Numerical Optimization*, 2nd ed.; Springer Science + Business Media LLC: New York, NY, USA, 2006; ISBN 978-0-387-40065-5.
42. Kullback, S.; Leibler, R.A. On Information and Sufficiency. *Ann. Math. Stat.* **1951**, *1951*, 79–86. [[CrossRef](#)]
43. Rolland, H.; Saintier, N.; Robert, G. Damage mechanisms in short glass fibre reinforced thermoplastic during in situ microtomography tensile tests. *Compos. Part B Eng.* **2016**, *90*, 365–377. [[CrossRef](#)]
44. Lenke, K. Kurzfaserverstärktes Polyamid—Charakterisierung der Mikroschädigungsentwicklung unter Zweiachsiger Mechanischer Last. Ph.D. Thesis, Technische Universität Berlin, Berlin, Germany, 2016.



© 2019 by the authors. Licensee MDPI, Basel, Switzerland. This article is an open access article distributed under the terms and conditions of the Creative Commons Attribution (CC BY) license (<http://creativecommons.org/licenses/by/4.0/>).